2016 IEEE International Conference on Advanced Intelligent Mechatronics (AIM)
Banff, Alberta, Canada, July 12–15, 2016

An Integrator-Backstepping Control Approach for Out-of-Plane Needle Deflection Minimization

Michael Waine[1], Carlos Rossa[1], Nawaid Usmani[2], Ron Sloboda[2] and Mahdi Tavakoli[1]

Abstract— **In this paper, we develop a needle steering strategy designed to reduce the out-of-plane deflection of a flexible, bevel-tipped needle for clinical needle insertion applications. This is performed through an integrator-backstepping approach. Integrator-backstepping is a nonlinear feedback controller design that divides the entire system into a sequence of smaller design problems that are easier to manage. Simulations were performed to observe the effects of our controller design on the system's response, specifically the rate at which the out-of-plane deflection converges. We tested our proposed method using a biological tissue phantom composed of two separate heterogeneous layers and using an 18 gauge brachytherapy needle. A paired-sample t-test was performed to compare out-of-plane needle deflection results with and without the use of our needle steering algorithm under varying bevel-angle starting conditions. Results showed a significant decrease in the out-of-plane needle deflection with the use of our controller at the 1% significance level. The absolute-mean out-of-plane needle deflection at a depth of 140 mm changed from 7.1 mm to 0.7 mm with the implementation of our needle steering approach. Our proposed steering method does not require "drilling" motions often encountered in duty-cycling controllers, and has been shown to be effective for clinical needles travelling through multiple heterogeneous tissue layers.**

I. Introduction

The use of bevel-tipped needles has been an integral component of many widely-performed medical procedures, such as the use of hypodermic needles for injecting medications or sampling fluids from the body, and the use of brachytherapy needles for administering internal radiation therapy. Typically, these needles have a hollow interior, allowing for fluids or medications to be ejected, while still maintaining a sharp edge that can be advanced easily through multiple, heterogeneous tissue layers [1].

A major issue related to the use of bevel-tipped needles is that the asymmetrical tip leads an imbalance of forces applied to the leading edge of the needle, as shown in Fig. 1, causing the needle to deflect during insertion. However, this characteristic can be exploited: by rotating the needle axially, the orientation of the resultant needle-tip forces can be controlled and used to provide steering capabilities.

This work was supported by the Natural Sciences and Engineering Research Council (NSERC) of Canada under grant CHRP 446520, the Canadian Institutes of Health Research (CIHR) under grant CPG 127768, and by the Alberta Innovates - Health Solutions (AIHS) under grant CRIO 201201232.

[1]Michael Waine (corresponding author), Carlos Rossa and Mahdi Tavakoli are with the Department of Electrical and Computer Engineering, University of Alberta, AB, Canada T6G 2V4. E-mail: mwaine@ualberta.ca; rossa@ualberta.ca@ualberta.ca; mahdi.tavakoli@ualberta.ca

[2]Nawaid Usmani and Ron Sloboda are with the Department of Oncology, University of Alberta, Edmonton, AB, Canada T6G 1Z2. E-mail: {nawaid.usmani, ron.sloboda}@albertahealthservices.ca.

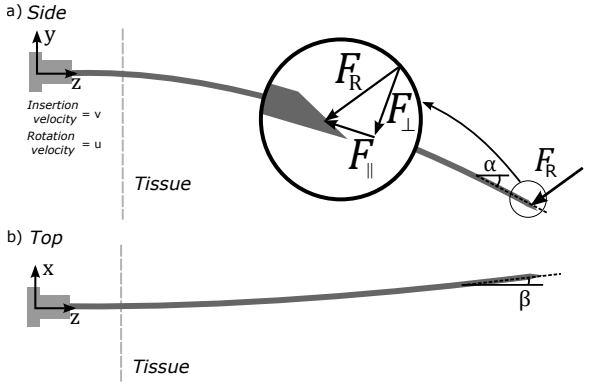

Fig. 1. Depiction of a bevel-tipped needle with views from the a) side and b) top. The $y-z$ plane represents the in-plane needle deflection. $F_\parallel$ represents the forces parallel to the deflected needle shaft, $F_\perp$ represents the forces perpendicular to the deflected needle shaft, and F_R represents the resultant of these two forces.

There have been a variety of studies performed on needle steering and the development of needle steering robots. For example, the needle steering robot developed by Neubach et al. [2] made use of a spring-based interaction model. DiMiao and Salcudean [3] developed a system that made use of repulsion and attraction potentials to steer the needle and Abayazid *et al.* [4] developed both a kinematics and mechanics-based steering algorithm. In these studies, the needle has been assumed to remain in a single plane throughout the insertion process. However, factors such as tissue deformation can influence the needle's trajectory and lead to out-of-plane deflection. As well, out-of-plane deflection is nearly inevitable unless the needle is completely stopped during the rotation process.

Some research groups have focused on developing 3D needle steering algorithms. Groups including Fichtinger *et al.* [5] and Salcudean *et al.* [6] have relied on laterally adjusting an external needle guide template to affect the needle's trajectory during the insertion process. These type of surgical robots take up a lot of space, which may not always be available in the operating room. Many other groups have focused on the use of needle rotation to perform robot-assisted needle steering. Many groups in this area have focused on experiments utilizing very thin, nitinol wire as opposed to clinical needles, such as Vrooijink *et al.* [7], Adebar *et al.* [8], and Jur van den Berg *et al.* [9]. As well, [7]-[10] make use of duty-cycling controllers, in which the needle is inserted with periods of no rotation or periods of continuous rotation, sometimes with rotation velocities of up

to five rotations per second [7]. It is our desire to reduce this type of "drilling" motion, since it could have significant effects on tissue trauma, swelling, and recovery. Instead, we want to focus on controlled, smaller-scale, slower rotations performed throughout the insertion process.

The contributions of this paper include the development of a control algorithm designed to minimize deflection in the horizontal $x-z$ plane and force the needle to deflect primarily in the $y-x$ plane. Our proposed method makes use of an integrator-backstepping approach to develop a needle steering algorithm. Integrator-backstepping is a nonlinear design tool based on the proper selection of a Lyapunov function. The design problem is segmented into several smaller, cascaded subsystems that are easier to solve and fine-tune [11]. The control algorithm we used is based on the well-studied bicycle model, developed in [12]. We avoid the use of drilling motions often encountered in duty-cycling control approaches, and instead rely on more regulated, smaller-scale, lower velocity needle steering motions to reduce the negative effects of the steering algorithm on tissue. Although the relationship between needle rotation, tissue trauma, edema, and tissue recovery has not been covered extensively in the literature, from a clinical perspective it is reasonable to err on the side of caution to reduce exposing patients to unnecessary harm. Our study involves the use of *ex-vivo* biological tissue samples rather than artificial tissue phantoms like agar or gelatin. We also focus on the use of clinical brachytherapy needles, instead of nitinol wire. The deflection of the needle is monitored through the use of 2D ultrasound (US) images. Our choice of the tissue phantoms, needles, and imaging methods used in our experiments are intended to improve the clinical relevance of our study. Our goal is to demonstrate a novel and effective controller design that can be used to reduce out-of-plane deflection during percutaneous needle insertion procedures.

The rest of the paper is structured as follows. Section II describes the development of our needle steering control algorithm. Section III gives an overview of the experimental setup used to test our method. Simulation and experimental results are shown in Section IV and are discussed in Section V. Conclusions are drawn in Section VI.

II. Controller Design

In this section, we discuss the derivation of our control approach, based on the nonlinear controller design technique known as integrator-backstepping. In Section II-B, we will derive the control input equations necessary for reducing deflection in the horizontal $x-z$ plane, and restricting the needle to deflect primarily in the $y-z$ plane. We refer to this as Vertical Deflection Control, since the majority of needle deflection is constrained to the vertical plane. We also detail the control logic used to handle special case scenarios in Section II-C.

A. Needle Steering Control Using Integrator-Backstepping

The kinematic equations for a flexible bevel-tipped needle used in this paper was based on the bicycle model developed by Webster *et al.* [12] and derived in its current-form in by Kallem and Cowan [13]. The equations are shown below.

$$\begin{bmatrix} \dot{x} \\ \dot{y} \\ \dot{z} \\ \dot{\alpha} \\ \dot{\beta} \\ \dot{\gamma} \end{bmatrix} = \begin{bmatrix} \sin\beta & 0 \\ -\cos\beta\sin\alpha & 0 \\ \cos\alpha\cos\beta & 0 \\ \kappa\cos\gamma\sec\beta & 0 \\ \kappa\sin\gamma & 0 \\ -\kappa\cos\gamma\tan\beta & 1 \end{bmatrix} \begin{bmatrix} v \\ u \end{bmatrix} \tag{1}$$

The values x, y, and z refer to the position of the needle tip, while α, β, and γ refer to the yaw, pitch and roll of the needle respectively. The bevel orientation shown in Fig. 1 is at $\gamma = 0^\circ$. The dot operator $\{\dot{}\}$ represents the first derivative with respect to time. The maximum deflection of the needle is defined by a radius of curvature κ. The values v and u refer to the insertion velocity and axial rotation velocity of the needle respectively, both of which are applied to the base of the needle by our needle steering robot. The variable u is the control input, and we assume that $v \geq 0$, since (4) is only valid for forward insertion of the needle, as opposed to needle retraction [12]. In this particular study v is held constant throughout the entire insertion.

In the integrator backstepping approach, a stabilizing control input can be found for a system of the form

$$\begin{aligned} \dot{x} &= f(x) + g(x)\xi_1 \\ \dot{\xi}_1 &= f_1(x,\xi_1) + g_1(x,\xi_1)\xi_2 \\ \dot{\xi}_2 &= f_2(x,\xi_1,\xi_2) + g_2(x,\xi_1,\xi_2)u \end{aligned} \tag{2}$$

where x, ξ_1 and ξ_2 represent the state variables and u represents the control input.

A control law that stabilizes the above system to the origin can be calculated using the following equation [11]

$$u = \frac{1}{g_2}\left\{\frac{\partial\phi}{\partial x}(\dot{x}) + \frac{\partial\phi}{\partial\xi_1}(\dot{\xi}_1) - \frac{\partial V}{\partial\xi_1}g_1 - k[\xi_2 - \phi] - f_2\right\} \tag{3}$$

where ϕ and V are the stabilizing control law and associated Lyapunov function for the system comprised of (2) while treating ξ_2 as an independent input. The value k is a tunable gain parameter, with $k > 0$.

B. Vertical Deflection Control

In order to limit the needle to the vertical plane, thereby reducing deflection in the horizontal plane, we must develop a control input that brings x and β to zero. This can be performed by applying integrator-backstepping to the following system:

$$\begin{bmatrix} \dot{x} \\ \dot{\beta} \\ \dot{\gamma} \end{bmatrix} = \begin{bmatrix} \sin\beta & 0 \\ \kappa\sin\gamma & 0 \\ -\kappa\cos\gamma\tan\beta & 1 \end{bmatrix} \begin{bmatrix} v \\ u \end{bmatrix} \tag{4}$$

Let us use the change of variable $\xi_1 = \sin\beta$ and $\xi_2 = \sin\gamma$. Then we can re-write (4) as:

$$\begin{bmatrix} \dot{x} \\ \dot{\xi}_1 \\ \dot{\xi}_2 \end{bmatrix} = \begin{bmatrix} \xi_1 & 0 \\ \pm\kappa\xi_2\sqrt{1-\xi_1^2} & 0 \\ \frac{\mp\kappa\xi_1(1-\xi_2^2)}{\sqrt{1-\xi_1^2}} & \pm\sqrt{1-\xi_2^2} \end{bmatrix} \begin{bmatrix} v \\ u \end{bmatrix} \tag{5}$$

The above system is now in strict feedback form. After one iteration of integrator-backstepping, performing the change of variables $\eta = \xi_1 + x$, we use the equations for $\dot{x}$ and $\dot{\xi}_1$ from (5) to obtain the following system:

$$\begin{bmatrix} \dot{x} \\ \dot{\eta} \end{bmatrix} = \begin{bmatrix} \eta - x & 0 \\ \pm\kappa\xi_2\sqrt{1-(\eta-x)^2} & 0 \end{bmatrix} \begin{bmatrix} v \\ u \end{bmatrix} \tag{6}$$

Choosing the Lyapunov function

$$V_1 = \frac{1}{2}x^2 + \frac{1}{2}\eta^2 \tag{7}$$

$$\dot{V}_1 = -v\left[x^2 - \left(\eta^2 \pm \kappa\eta\xi_2\sqrt{1-(\eta-x)^2}\right)\right] \tag{8}$$

and viewing ξ_2 as an independent input for the system in (6), we can find a state feedback control law $\xi_2 = \phi(x,\eta)$ to stabilize the system to the origin $(x, \sin\beta, \sin\gamma) = (0,0,0)$. Here, $\gamma = 0$ is the same bevel-angle orientation shown in Fig. 1. With respect to (6), a stabilizing control law can be selected as:

$$\phi(x,\xi_1) = -2\frac{\eta}{\pm\kappa\sqrt{1-\xi_1^2}} \tag{9}$$

Using (3), and performing the substitutions $\pm\sqrt{1-\xi_1^2} = \cos\beta$ and $\pm\sqrt{1-\xi_2^2} = \cos\gamma$, a stabilizing control law u for the system described in (5) is

$$u = -\frac{v}{\cos\gamma}\left(\frac{2\tan\beta}{\kappa} + \frac{2\sin\gamma}{\cos^2\beta} + \kappa\cos\beta(\sin\beta + x) + \frac{k}{v}\left[\sin\gamma + \frac{2(\sin\beta + x)}{\kappa\cos\beta}\right] - \kappa\cos^2\gamma\tan\beta\right) \tag{10}$$

where $k > 0$. The corresponding Lyapunov function is:

$$V_2 = \frac{1}{2}x^2 + \frac{1}{2}(\sin\beta + x)^2 + \frac{1}{2}\left(\sin\gamma + \frac{2(\sin\beta + x)}{\kappa\cos\beta}\right)^2 \tag{11}$$

Note that in (10) and (11) there are discontinuities at $\beta = \{90^\circ + (180^\circ)n,\ n \in \mathbb{Z}\}$ and $\gamma = \{90^\circ + (180^\circ)n,\ n \in \mathbb{Z}\}$. In the following section, we discuss the meaning of these discontinuities and develop a revised control logic to handle operating near these discontinuities, specifically values of γ that cause (10) to diverge towards infinity.

C. Control Logic for Special Cases

Based on the control law derived in (10), we need to develop strategies to handle points like $\gamma = \{90^\circ + (180^\circ)n,\ n \in \mathbb{Z}\}$ and $\beta = \{90^\circ + (180^\circ)n,\ n \in \mathbb{Z}\}$ where the control law tends towards infinity. With respect to β, these discontinuities occur when the needle's orientation is perpendicular to the $y-z$ plane. In practice, we want to perform corrective actions long before the needle reaches this state, so this issue is not likely to occur and is not of great concern, especially with the 18 gauge brachytherapy needles used in our paper. More concerning is the issue with γ: discontinuities occur whenever the needle's bevel angle aligns with the $x-z$ plane. We have developed a strategy to handle cases were the controller guides γ towards these discontinuities.

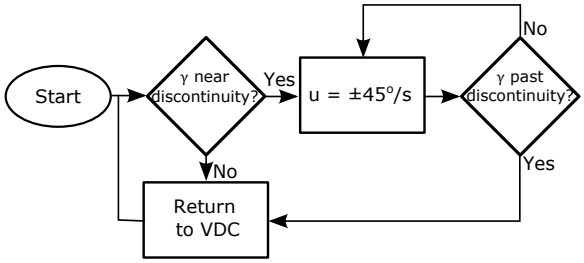

Fig. 2. Control logic used during instances where γ is near discontinuous.

We monitor γ, assuming that the bevel angle of the needle's tip is the same as the angle recorded by the encoder at the needle's base. This assumption disregards the effects of torsional friction applied to the needle shaft, which should be quite small in practice [12]. As long as γ is further than 3° from one of the discontinuities, u is controlled via (10). If γ is within 3° of one of the discontinuities, we simply apply a constant $u = \pm 45^\circ$/s to push γ past the discontinuity by 3° and re-apply (10). For example, if γ approaches 87°, u is controlled to bring γ to 93° and (10) is re-instated. A summary of this control logic is shown in Fig. 2.

III. Experimental Setup

The experimental setup used in this paper is similar to the one described in our past work [14]. The setup is comprised of a two degree-of-freedom robot; a prismatic joint is connected to a needle carriage, which holds the needle in place as it is inserted into tissue. A rotational joint is used to rotate the needle during insertion and is our needle steering input described in (10). An ultrasound probe is attached to a separate motor, which is controlled to match the insertion velocity of the needle so that the needle tip can be observed throughout the entire insertion process.

In all of our experiments, we used a dual-layer biological tissue phantom composed of pork tissue and beef tissue in order to test the effects of our needle steering control law on multiple heterogeneous biological tissue layers. The intent was to create a phantom tissue similar to the clinical conditions encountered during permanent prostate brachytherapy, where the needle must traverse through an initial connective tissue layer before traveling through the prostate. The first 100 mm of the tissue phantom was composed of pork tissue, and the final 70 mm of the phantom was composed of beef tissue. An 18 gauge brachytherapy needle was used for each of the needle insertion trials. The insertion velocity was set to 10 mm/s and the rotation velocity was limited to a maximum of $\pm 180^\circ$/s. By limiting the maximum rotation velocity, we intend to reduce the energy and heat that the control motions apply to the tissue. However, a more in depth study of the relationship between tissue trauma and needle rotation is a subject for future work.

A depiction of our experimental setup is shown in Fig. 3. In order to track the needle under ultrasound feedback, we implemented an image processing algorithm incorporating a

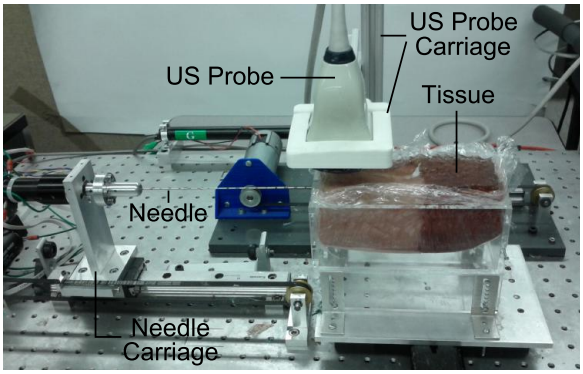

Fig. 3. Experimental Setup. A two degree-of-freedom needle insertion robot is used to test our algorithm. A prismatic joint which controls the position of the needle carriage allows the robot to insert the needle into the tissue. A rotational joint allows the robot to rotate the needle during insertion. An US probe is attached to a separate motor that is used to track the needle tip over the course of the insertion.

dynamic region-of-interest, along with a threshold-based needle tracking approach. The details of the image processing algorithm are discussed further in [14].

IV. Results

A. Simulation Results

Simulations are performed in Simulink to test the effects of adjusting the gain k derived in (10) on convergence time. We define convergence time as the time taken for the x deflection to settle to within 0.5 mm of its target (which is zero in our study).

The simulations were performed using $\kappa = 1/r$, with $r =$ 500 mm. This is the upper end of needle deflection observed in preliminary *ex-vivo* biological tissue trials performed in our lab using an 18 gauge brachytherapy needle. The maximum insertion depth was set to 200 mm and the insertion velocity was held constant at 10 mm/s.

Based on the results shown in Fig. 4, for half of the results (initial values of: $[x,\beta,\gamma] = [0,0,90],[1,0,0],[1,0,90]$), increasing the gain decreases the convergence time. However, the increase in convergence time is negligible after $k \geq 0.6$. For the remainder of the simulated starting conditions, as the gain is increased, the convergence time decreases until $k = 0.4$ to 0.6. After this point, increasing k has a detrimental effect on the convergence time. A gain value between 0.5 and 0.6 offers a reasonable convergence rate for a wide variety of starting conditions. In this paper, for the experiments discussed in Section IV-B, we used a gain of $k = 0.6$.

B. Experimental Results

We performed experiments observing deflection results along the x-axis using no needle steering and compared this with the implementation of our proposed control approach. The initial value of γ was manipulated by 45° increments for each successive trial, while the x, y, α and β values were initialized to their 0 values. Each experiment consisted of eight separate trials for bevel angles γ ranging from 0°

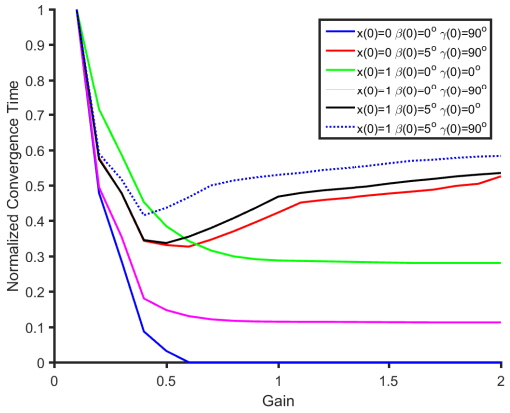

Fig. 4. Simulation Results. The comparison of gain k to convergence time is shown. The graph compares the results over a number of different starting conditions with respect to the needle's initial position (in mm) and/or orientation (in degrees). For example: $x(0) = 1$ $\beta(0) = 5°$ $\gamma(0) = 90°$ represents the situation where the needle's initial x position was translated 1 mm to the right of the target location, its initial β orientation was rotated $+5°$ with respect to the target location, and its bevel angle was set to 90°.

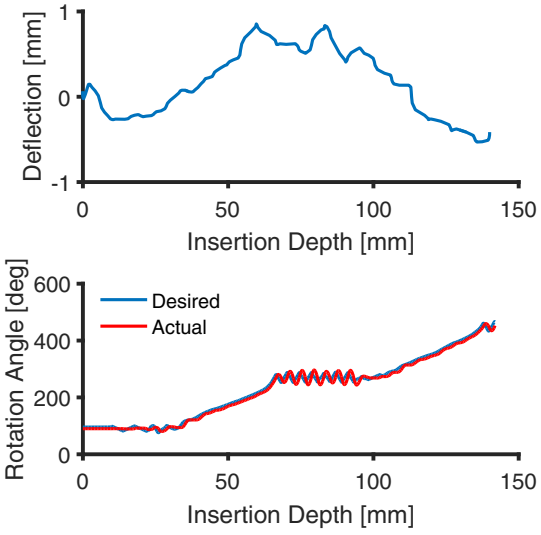

Fig. 5. An example of the a) out-of-plane deflection and b) rotation angle as a function of depth. In b), "Desired" represents the desired bevel angle while "Actual" represents the measured bevel angle. The needle's bevel angle was initialized to 90°.

to 315°. For each of these bevel angles, one trial without needle steering and two trials implementing our proposed method were performed, resulting in 24 insertions in total. A comparison of the out-of-plane deflection and the needle's rotation angle as a function of the insertion depth is shown in Fig. 5. The needle's initial bevel angle was 90°. Out-of-plane deflection results at the needle's maximum insertion depth of 140 mm are shown in Table I.

Using the results shown in Table I, we performed a paired-sample t-test to compare the out-of-plane needle deflection results with and without the use of our proposed needle

TABLE I

COMPARISON OF PLANAR DEFLECTION USING NO STEERING AND THE PROPOSED CONTROL APPROACH (STEERING)

Trial	Bevel Angle	Deflection [mm]		
		No Steering	Steering	
1	0	-2.7	-0.9	-0.8
2	45	-8.1	-1.2	0.8
3	90	-10.0	-0.1	1.0
4	135	-9.3	0.6	0.9
5	180	1.3	0.9	1.0
6	225	7.2	0.3	-0.3
7	270	11.5	-0.4	-0.1
8	315	7.0	-1.3	-0.6

TABLE II

SUMMARY OF PAIRED-SAMPLE T-TEST STATISTICS

	No Steering	Steering Set 1	Steering Set 2
Abs. Mean Deflection [mm]	7.1	0.7	0.7
Standard Deviation [mm]	3.5	0.4	0.3
t Statistic	-	4.89	4.98
p Value	-	0.0018	0.0016

steering method. The "No Steering" trial set was compared with each of the "Steering" trial sets shown in Table I. The two "Steering" trial sets will be referred to as "Steering Set 1" and "Steering Set 2" throughout the discussion. A summary of the relevant statistics from the paired-sample t-test is shown in Table II.

From Table II, there was a significant decrease in out-of-plane deflection as a result of our proposed needle steering algorithm. The absolute mean deflection decreased from 7.1 mm for the No Steering trial set to 0.7 mm for Steering Set 1 and Steering Set 2. The absolute mean deflection for the entire set of needle steering trials was 0.7 mm. This represents an average decrease of 90% for the various bevel-angle starting conditions.

There was also a noticeable decrease in the variance of the out-of-plane deflection with the use of our proposed control method. The standard deviation of the absolute deflection results decreased from 3.5 mm for the No Steering trial set to 0.4 mm for Steering Set 1 and 0.3 mm for Steering Set 2. The standard deviation for the entire set of needle steering trials was 0.4 mm. The results show a 89% decrease in the out-of-plane deflection variance with the use of our proposed method.

The results of the paired-sample t-tests also showed a significant decrease in out-of-plane deflection in the Steering Sets at the 1% significance level. The t-test comparing the No Steering trial set with Steering Set 1 resulted in a t-statistic of 4.89 and a p-value of 0.0018. The t-test comparing the No Steering trial set with Steering Set 2 resulted in a t-statistic of 4.98 and a p-value of 0.0016. These results show that the use of our needle steering approach results in a significant decrease in the out-of-plane needle deflection compared to the results without the use of any type of needle steering.

V. DISCUSSION

Overall, the results show that our needle steering control algorithm can significantly decrease the out-of-plane deflection for percutaneous needle insertion procedures through a variety of heterogeneous tissue layers.

Fig. 5 shows a demonstration of our steering algorithm applied to an initial γ of 90°. When the out-of-plane deflection becomes large, the steering algorithm tends to guide γ towards the discontinuity points to quickly bring the needle back in-plane. Based on the control logic described in Section II-C, this causes the needle to hover near the discontinuity in a saw-tooth type pattern, as shown in Fig. 5.

The method proposed in this paper could have significance in clinical situations where the needle deflection should be reduced or controlled to within a single plane. For example, in prostate brachytherapy applications, where radioactive seeds must be implanted into the prostate gland with high precision, if the plane of needle deflection is known or restricted, then the brachytherapy seeds can be more accurately tracked and monitored, since their locations should remain in or near the plane of needle deflection. As well, if out-of-plane needle deflection is minimized, longitudinal ultrasound imaging, where the ultrasound array is parallel to the needle's long axis, could be used to greater effect. To be most effective, longitudinal ultrasound imaging relies on the needle remaining in a single plane. The use of our needle steering control algorithm could be used to achieve this in applications where longitudinal imaging may provide additional, useful information.

The out-of-plane deflection of our method was comparable to similar methods such as [10] and [13], despite our use of multiple heterogeneous layers. The use of a multi-layered tissue phantom allowed us to simulate clinical conditions encountered during permanent prostate brachytherapy, where the needle must traverse a combination of muscle, connective, and fatty tissue layers, along with the prostate gland itself. The effects of the tissue interface are not pronounced, as observed in Fig. 5, but similar effects are observed in clinical permanent prostate brachytherapy procedures, where surgeons cannot feel a significant difference between the connective tissue and the prostate gland layers during the procedure.

Currently, the proposed method is only designed to reduce out-of-plane deflection, with no control applied to the in-plane deflection. The next step is to develop a 3D needle steering control strategy to reduce deflection in both the $x-z$ and $y-z$ planes to a tolerable threshold. Inspiration for switching between the two planes will likely derive from gain-scheduling controllers, where scheduling variables are used to determine when to switch between various linear controllers. We expect that a similar approach can be applied to the initial needle steering control approach presented in this paper to develop a 3D steering method. Another consideration that must be taken into account is how to quantify and minimize tissue trauma. We plan to explore a

way to quantify tissue trauma by examining u and the total amount that the needle must be rotated in order to achieve our desired results.

VI. Conclusion

In this paper, we describe a method for controlling out-of-plane needle deflection through the use of an integrator-backstepping control approach. Our needle insertion setup consisted of a two degree-of-freedom surgical robot. The insertion velocity of the needle was set to a constant value of 10 mm/s and the rotation velocity of the needle was controlled via our derived algorithm to minimize the needle's deflection along the x-axis.

Simulations were performed in Simulink to test the effects of our controller gain on the system's convergence time. As well, experiments were performed using a dual-layered biological phantom tissue composed of 100 mm of pork tissue followed by 70 mm of beef tissue to simulate the different heterogeneous tissue layers encountered during clinical permanent prostate brachytherapy conditions. Twenty four needle insertion trials were performed under a variety of bevel-angle staring conditions ranging from 0° to 315°. Eight trials were performed without any needle steering and sixteen trials were performed with the use of our proposed method.

A paired-sample t-test was used to compare the out-of-plane needle deflection results with and without the use of our needle steering control algorithm under the different bevel-angle starting conditions. Results showed a significant decrease in absolute out-of-plane needle deflection with the use of our needle steering algorithm at the 1% significance level. The absolute mean needle deflection at the maximum insertion depth decreased from 7.1 mm to 0.7 mm through the use of our control approach.

Future work includes the development of a control approach designed to reduce needle deflection in both the $x-z$ and $y-z$ planes to below a tolerable threshold. This concept will likely incorporate ideas from gain-scheduling controllers in order to develop a control logic to switch control focus between the two different planes. As well, tissue characteristics could be incorporated into the needle steering control approach through real-time parameterization of κ. A method to compare the effects of the controller gain on potential tissue trauma will also be explored.

References

[1] J. P. Rathmell, *Atlas of image-guided intervention in regional anesthesia and pain medicine*. Lippincott Williams & Wilkins, 2011.

[2] Z. Neubach and M. Shoham, "Ultrasound-guided robot for flexible needle steering," *Biomedical Engineering, IEEE Transactions on*, vol. 57, no. 4, pp. 799–805, 2010.

[3] S. P. DiMaio and S. Salcudean, "Needle steering and motion planning in soft tissues," *Biomedical Engineering, IEEE Transactions on*, vol. 52, no. 6, pp. 965–974, 2005.

[4] M. Abayazid, R. J. Roesthuis, R. Reilink, and S. Misra, "Integrating deflection models and image feedback for real-time flexible needle steering," *Robotics, IEEE Transactions on*, vol. 29, no. 2, pp. 542–553, 2013.

[5] G. Fichtinger, J. P. Fiene, C. W. Kennedy, G. Kronreif, I. Iordachita, D. Y. Song, E. C. Burdette, and P. Kazanzides, "Robotic assistance for ultrasound-guided prostate brachytherapy," *Medical image analysis*, vol. 12, no. 5, pp. 535–545, 2008.

[6] S. E. Salcudean, T. D. Prananta, W. J. Morris, and I. Spadinger, "A robotic needle guide for prostate brachytherapy," in *Robotics and Automation, 2008. ICRA 2008. IEEE International Conference on*. IEEE, 2008, pp. 2975–2981.

[7] G. J. Vrooijink, M. Abayazid, S. Patil, R. Alterovitz, and S. Misra, "Needle path planning and steering in a three-dimensional non-static environment using two-dimensional ultrasound images," *The International Journal of Robotics Research*, pp. 1–14, 2014.

[8] T. K. Adebar, A. E. Fletcher, and A. M. Okamura, "3-D ultrasound-guided robotic needle steering in biological tissue," *Biomedical Engineering, IEEE Transactions on*, vol. 61, no. 12, pp. 2899–2910, 2014.

[9] J. Van Den Berg, S. Patil, R. Alterovitz, P. Abbeel, and K. Goldberg, "LQG-based planning, sensing, and control of steerable needles," in *Algorithmic Foundations of Robotics IX*. Springer, 2011, pp. 373–389.

[10] D. C. Rucker, J. Das, H. B. Gilbert, P. J. Swaney, M. I. Miga, N. Sarkar, and R. J. Webster, "Sliding mode control of steerable needles," *Robotics, IEEE Transactions on*, vol. 29, no. 5, pp. 1289–1299, 2013.

[11] H. K. Khalil and J. Grizzle, *Nonlinear systems*. Prentice hall New Jersey, 1996, vol. 3.

[12] R. J. Webster, J. S. Kim, N. J. Cowan, G. S. Chirikjian, and A. M. Okamura, "Nonholonomic modeling of needle steering," *The International Journal of Robotics Research*, vol. 25, no. 5-6, pp. 509–525, 2006.

[13] V. Kallem and N. J. Cowan, "Image guidance of flexible tip-steerable needles," *Robotics, IEEE Transactions on*, vol. 25, no. 1, pp. 191–196, 2009.

[14] M. Waine, C. Rossa, R. Sloboda, N. Usmani, and M. Tavakoli, "Needle tracking and deflection prediction for robot-assisted needle insertion using 2d ultrasound images," *Journal of Medical Robotics Research*, vol. In press, 2015.